Structure Development and Dynamics of Vibration Welding of Poly(ethylene naphthalate) from Amorphous and Semicrystalline Precursors

M. CAKMAK, J. ROBINETTE, S. SCHAIBLE

Polymer Engineering Institute, College of Polymer Engineering and Polymer Science, University of Akron, Akron, Ohio 44325-03010

Received 2 December 1997; accepted 23 January 1998

ABSTRACT: The influence of process conditions on the structural hierarchy developed in the heat-affected zone (HAZ) of polyethylene 2,6-naphthalene dicarboxylate (PEN) welded both from amorphous, as well as crystalline, precursors was studied using optical microscopy and a matrixing microbeam X-ray diffraction camera developed in our laboratories. The structural gradients developed in the HAZ were found to be highly dependent on welding conditions as well as on the state of crystallinity in the precursor samples. In the amorphous sample, the HAZ is composed of 2 distinct layers. The inner layer (II) (HAZ-II) is formed at the immediate vicinity of the original weld interface, and, within this region, the sample is highly oriented and crystallized. In the outer layer (I) (HAZ I), between this layer and the unaffected region, the polymer exhibit deformed zones, but little or no crystallinity is noticed. In HAZ-I, the polymer chains melt and deform significantly and crystallize upon cooling; and in the HAZ I, the polymer chains located in this region increase their temperature to reach temperatures $T > T_g$, where they are deformed under the dynamic forces generated at the weld interface as well as under the normal forces. Due to the low crystallizability of PEN chains, the material mostly remain amorphous at this location. In the HAZ, a wave-like interface was observed at the bothe HAZ-II and HAZ I boundaries. This was attributed to the presence of 2 regions of deformable bodies of large difference in viscosities which, in the presence of oscillatory stress field, results in wavy interface. The structural analysis revealed that as a result of significant shearing, the naphthalene planes are oriented parallel to the weld interface resembling graphitic structure. This had a detrimental effect on the mechanical performance of the parts, particularly in those samples welded from amorphous precursors. The samples welded from crystalline precursors exhibited more traditional HAZ structure gradient, and the boundary between the heat-affected and unaffected region is rather diffuse reflecting the rather broad nature of the melting temperature range in this polymer due to dynamic temperature gradient developed during and after the vibration stage. © 1998 John Wiley & Sons, Inc. J Appl Polym Sci 70: 89–108, 1998

Key words: HAZ; PEN; optical microscopy; crystallinity; welding

INTRODUCTION

Although there has been considerable research published on various aspects of vibration welding,[1–4] issues to clarify still remain, particularly pertaining to the evolution of structural gradients in the HAZ. There are some studies to elucidate the HAZ structure of some polymers, such as PP[5] and PBT[6] as they are related to process variables, and a considerable gap in the understanding of preferential orientation devel-

Correspondence to: M. Cakmak.

Journal of Applied Polymer Science, Vol. 70, 89–108 (1998)
 CCC 0021-8995/98/010089-20

opment in the HAZ region of the vibration welded parts still remains.

We have developed an instrumented vibration welding machine to investigate the influence of polymer type, state of structure and phase, and filler shape and type welding conditions on the welding behavior of various polymers,[7] including polyethylene 2,6-naphthalene dicarboxylate (PEN). This slow crystallizing polymer can be quenched into amorphous state during injection molding, or it can exhibit three-layer amorphous–shear-crystallized-amorphous structural gradients when molded, particularly into cavities of small dimensions where the polymer melt undergoes rapid cooling and shearing during the filling stage.[8] It can also be obtained in substantially crystalline state by molding into high mold temperatures or annealing the amorphous precursors at temperatures where thermal crystallization rates are high (150–220°C). We have found that the naphthalene planes orient parallel to the broad surfaces of the molded parts. The shear crystallized regions were found to be composed of α,[9] as well as higher melting β,[10] crystalline forms.

In the following, we present our results on the welding behavior of PEN from amorphous as well as semicrystalline precursors.

MATERIALS AND EXPERIMENTAL PROCEDURES

Polyethylene 2,6-naphthalene dicarboxylate (PEN) of 0.825 dL/gm IV, was provided by Goodyear Polyester Division (now Shell Polyester, Akron, OH). The pellets were dried overnight in a vacuum oven set at 150°C. The molded parts were produced using a Van Dorn 55-ton injection molding machine equipped with a standard ASTM cavity set with 0.635 × 1.27 × 6.35 cm rectangular prism end-gated cavity. The temperature profile of 232, 268, and 290°C was used along the barrel. An injection speed of 16.9 cm/s and mold temperature of 24°C was used for all the samples molded. After a holding time of 1 min in the mold, the samples were ejected from the machine. The molded samples were found to be transparent and free of shear crystallized layers.

For welding studies, we chose to use a 0.635 × 1.27 × 6.35 cm (0.25 × 0.50 × 2.5 in) rectangular prism, end-gated, ASTM sample. All of the as-molded samples were found to be free of shear

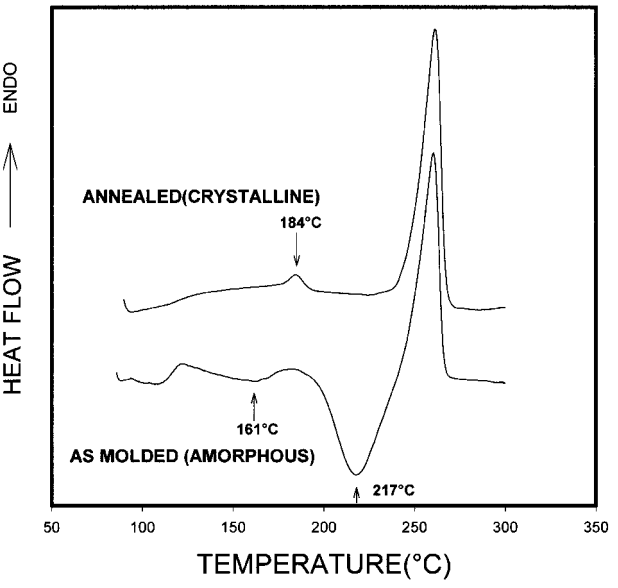

Figure 1 DSC curves of as-molded amorphous and constrained annealed (180°C, 3 h) semicrystalline PEN sample.

crystallized layers and uniformly amorphous. In order to obtain the crystalline samples, the as-molded amorphous samples were annealed at 180°C under vacuum for about 3 h. During this annealing process, samples were constrained in their width and thickness directions in specially designed, flat-faced clamps to preserve their geometrical integrity. The differential scanning calorimetry (DSC) curves of both the as-molded sample and the crystallized samples are shown in Figure 1. The Perkin–Elmer DSC-7 was used for these measurements at a heating rate of 20°C/min. As this figure indicates, the T_g is around 120°C, and we observe two cold crystallization peaks, one situated at 161°C and the other at 217°C. The lower crystallization peak is associated with the oriented amorphous chains in the injection-molded sample that crystallize upon heating in the DSC. The annealed sample show two endothermic peaks: one characteristically just above the annealing temperature (184°C); the other is the main melting peak.

Welding Conditions

The overall three-dimensional depiction of the vibration welding machine developed in our laboratories[7] is presented in Figure 2. A 15 Hp hydraulic power unit is connected to the 1.25 cm maximum amplitude servo actuator that drives the

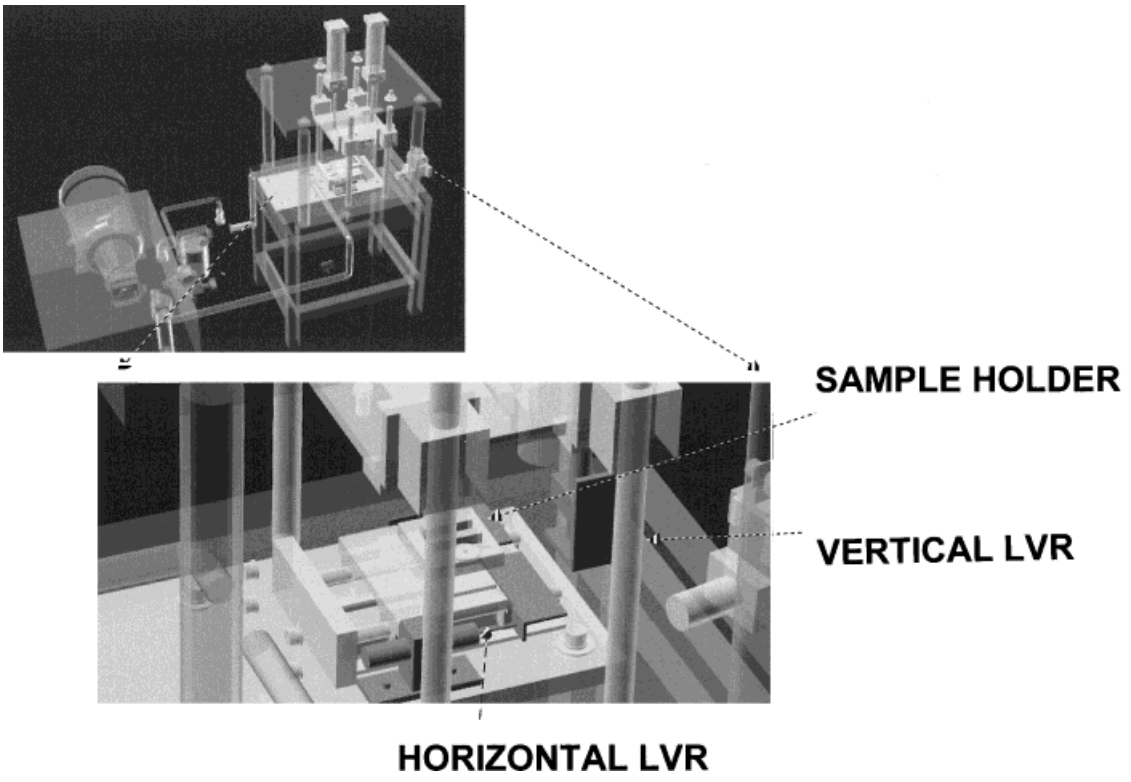

Figure 2 Solid rendering of the instrumented vibration welder.

samples mounted (wedge collar type) on a lower sample holder clamped onto a linear motion table. The second sample holder is mounted on the top moving platen that rides 4 linear bearings on 4 vertical 1-in diameter steel shafts. Two hydraulic pistons separately connected to the hydraulic power unit drive the top platen. A linear variable resistor (LVR) mounted vertically to measure the relative motion of the upper platen with the lower surface of the frame. The normal force, exerted by the hydraulic cylinder, is measured by a donut-shaped piezoelectric force transducer mounted in a recess located in the bottom of the upper platen. The frequency (and number of total cycles) of vibration was monitored via an infrared (IR) optical transducer mounted on the lower sample holder. A horizontally mounted LVR provided the amplitude of oscillations. The operating range of the welding machine 33–120 Hz and 0.55 mm (at 120 Hz) minimum amplitude and 3.5 mm (at 33 Hz) maximum amplitude.

The data acquisition was performed through the sensors of the machine that are connected to a data acquisition system, as well as to the control panel. The sensors described above are connected to Metrabyte DASH-8 data acquisition card mounted on a PC. The data was acquired using the Labtech Notebook software.

Cutting Procedures

The molded samples were cut in half by a band saw and subsequently polished using 400-grit sand paper, on an Ecomet polisher, with a sample holder designed to polish multiple samples simultaneously. This polishing step was performed in order to start each experiment with perfectly polished surfaces to provide consistent results.

Analysis

In order to investigate the evolution of structure in the HAZ, the welded samples were cut in the following two mutually perpendicular planes: one along the symmetry midplane in the direction of vibration designated as *X*-cut, and the other along the second symmetry midplane with its surface normal to the vibration direction, called *Y*-cut, as shown in Figure 3. We used a slow speed diamond saw for cutting 0.3-mm and 0.2-mm thick samples from initially amorphous and initially crystalline samples, respectively.

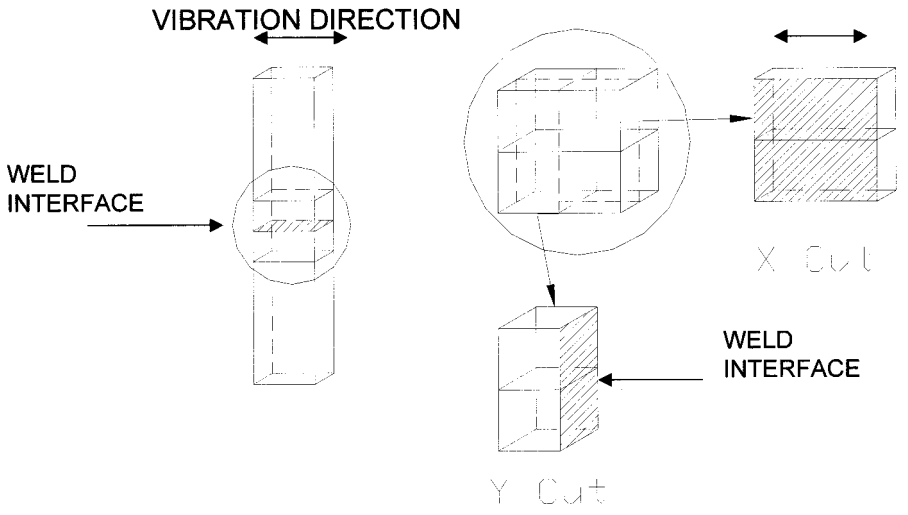

Figure 3 Cutting procedures *X* and (along vibration direction) *Y* (across the vibration direction).

Optical microscopy was performed on the *X*- and *Y*-cut samples using Laborlux 12 POL 5 optical microscope, equipped with a SONY 3 chip CCD camera, under cross-polarized light and digitized using Sun 4/150 workstation equipped with image digitization system. An *X*-*Y* stage was used to move the samples linearly across the weld, so that progressive images could be recorded, and then digitally combined together to obtain full image across the width of the samples.

A 12-kW Rigaku rotating anode X-ray generator equipped with a microbeam wide-angle X-ray scattering (WAXS) camera was used to take a series of WAXS patterns across the HAZ of the X-cut samples with the X-ray beam directed normal to the vibration direction. The generator was operated at 40 kV and 150 mA. The X-rays generated at the copper target was monochromatized using a nickel foil filter. The X-ray diffraction (XRD) patterns were taken at a series of sequential locations across the HAZ with 100-μm steps. A typical exposure time of 1 h was used.

Mechanical Testing

An Instron 4024 tensile tester with 50 KN load cell was used to test the samples following the ASTM D-638 method. A crosshead speed of 10 mm/s was used.

RESULTS

The Kinematics of Welding

As indicated in various publications in the past,[8,11,12] low mold temperatures generally result in little or no crystallinity in PEN, while the mold temperatures at 150–220°C can result crystallinities as high as 45–55% due to thermally activated crystallization. The first goal of this research program was to investigate the influence of precursor structure on the kinematics of the welding and the resulting structure and properties of the parts. The kinematics of welding was studied using the instrumented vibration welding machine designed and built in our group.[7] The original design of this machine was modified as part of this research to power the vertical axis with hydraulic power and additional accumulators to maintain dynamic stability of vibration motion during the course of the welding process. The results are shown in Figures 4 and 5 for 517 and 1035 kPa normal pressure, respectively. The frequency of 66 Hz and amplitude of 1.9 mm was kept constant for these studies. Although frequency is selected from the control panel, it is also sensed with optical detector to verify that it reaches the set value and remains constant for the duration of the experiment. In these curves, the frequency channel is plotted uncalibrated as

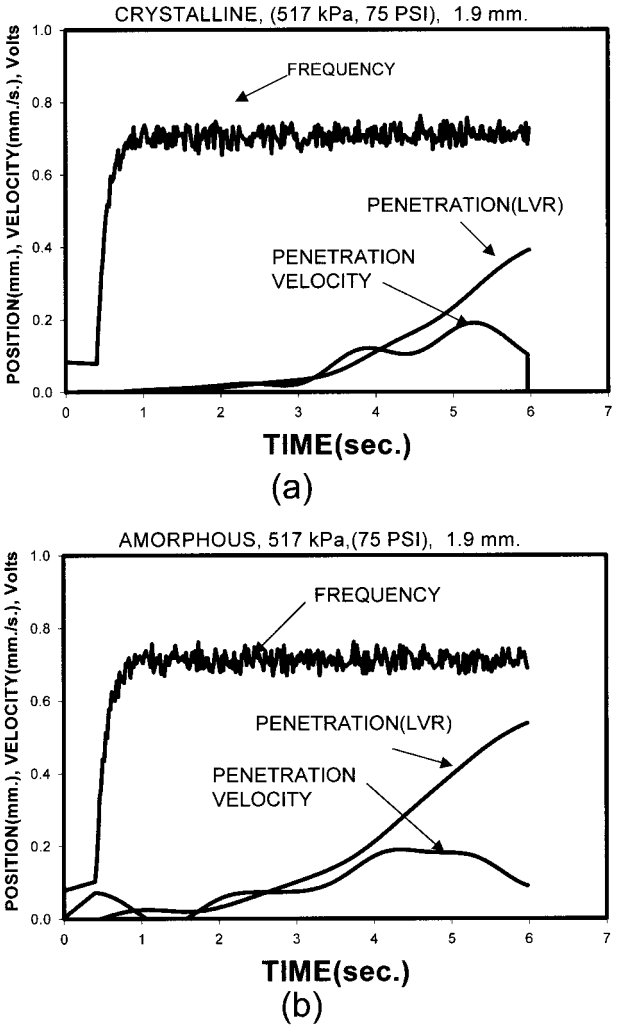

Figure 4 Dynamic data obtained at 517 kPa (75 psi) for (a) crystalline and (b) amorphous samples.

volts. It reaches rapidly to preset value within approximately 0.25 s and remains constant for all measurements reported here. The main differences between the amorphous and crystalline samples are observed in Figure 4. That is, the penetration starts much earlier in the initially amorphous precursor as compared to the crystalline PEN. This is a rather obvious result as the crystalline samples need to reach the melting range located at much higher temperatures, ~ 240–260, before they begin to flow; whereas the amorphous sample needs to reach temperatures just above 120°C, where it begins to behave rubbery and is able to deform under the stress field, imposed by the welding process. In Figure 4, we also plot the penetration velocity derived from the penetration distance obtained online. In this, there appears to be two plateaus, indicating two different slopes on the penetration curves. At high normal pressure (1034 kPa), aside from the expected increase in penetration rates, the differences in the penetration rate for initially amorphous and initially crystalline samples become quite clear. The amorphous samples exhibit almost double the rate of penetration exhibited by the crystalline samples. This is even more apparent in Figure 6. A comparison of Figure 6(a) with 6(b) also reveals that the slopes of these position (penetration) versus time curves are much more sensitive to the changes in normal pressure in the amorphous samples.

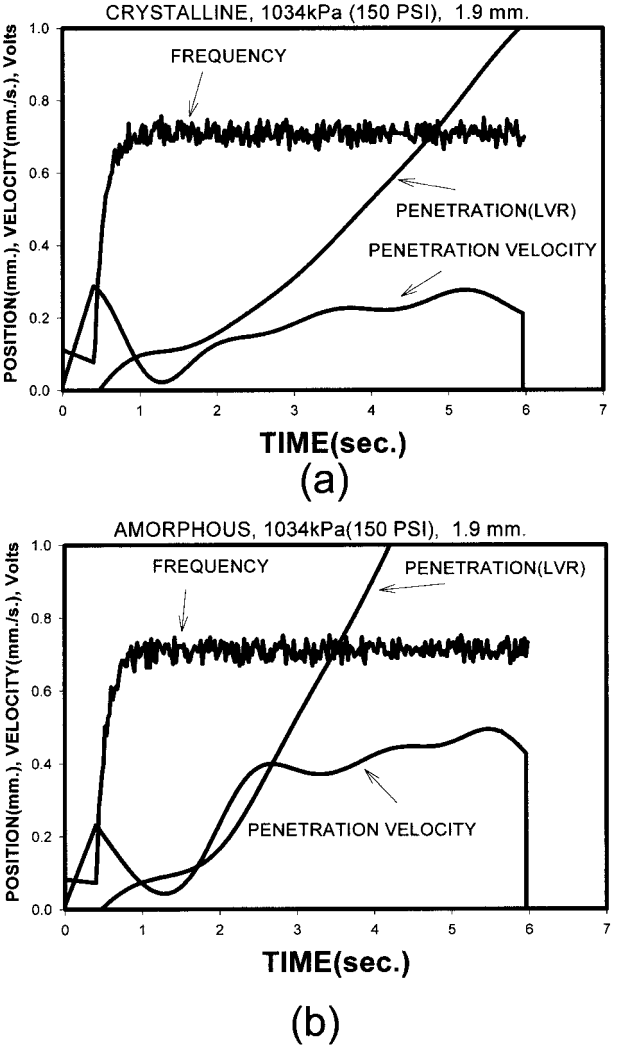

Figure 5 Dynamic data obtained at 1034 kPa (150 psi) for the (a) annealed (crystalline) sample and the (b) as-molded (amorphous) sample.

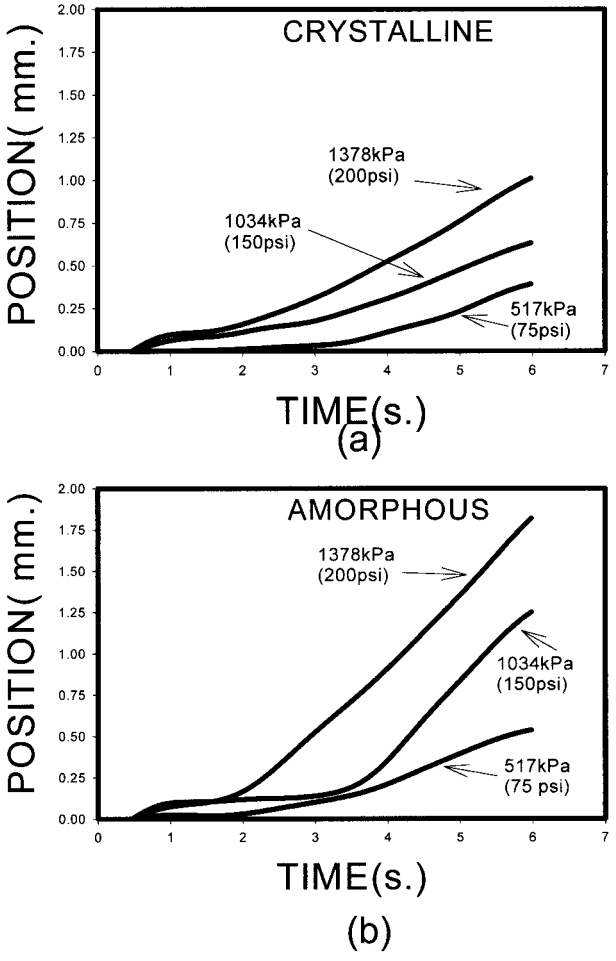

Figure 6 Penetration position versus time for various normal pressures for (a) annealed (crystalline) and (b) as-molded (amorphous) samples.

WELDING STAGES

Welding from Amorphous Precursors

In order to understand the time evolution of the welding process, we have welded a series of the samples for a specific number of cycles under the same frequency, amplitude, and normal pressure. A typical reflection optical photograph of the interface after 10 and 20 cycles are shown in Figure 7. It is quite noteworthy that the initiation of welding process is a very highly localized phenomenon, as evidenced by observing the contact surfaces. The lighter colored regions of elliptical shape (indicated by arrow) are regions where the interface begins to melt probably nucleated from small asperities, despite the fact that the sample surfaces are polished. The polishing marks are evident as faint diagonal lines in the direction

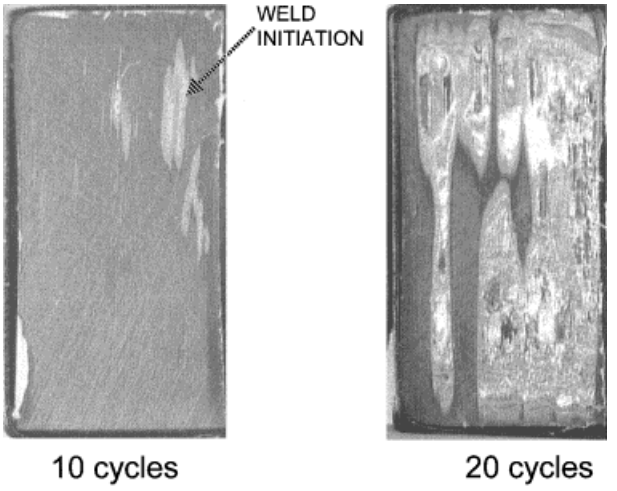

Figure 7 Time-sliced weld surfaces after break: frequency, 66 Hz; amplitude, 1.9 mm; normal pressure, 689 kPa (100 psi); amorphous PEN.

from lower left to upper right of the sample. In addition, one observes long thin scratch-like marks on other quadrants of the sample surface, representing very early stages of weld initiation. The surface representing 20 cycles clearly indicates the localized nature of weld initiation, and these elongated regions simply extend in the direction of vibration. In order to investigate the three-dimensional evolution of these weld initiation zones, we cut the samples using the *Y*-cut

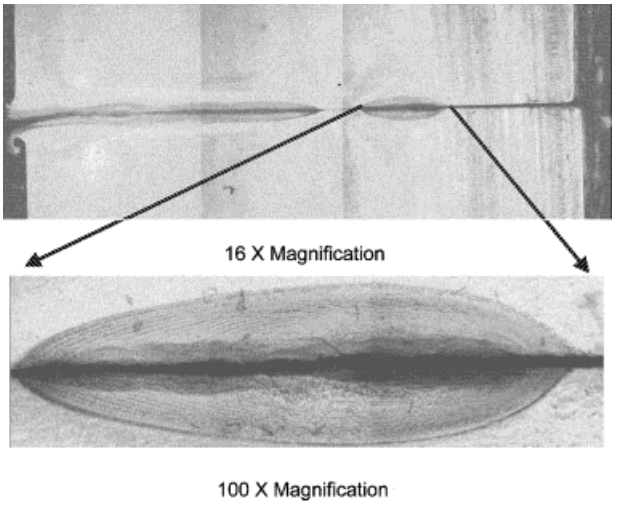

Figure 8 Transmission photomicrographs showing the *Y*-cut (normal to the vibration direction) sample at locations where the localized welding started (weld conditions: frequency, 66 Hz; amplitude, 1.9 mm; pressure, 690 kPa; 50 cycles; amorphous PEN.

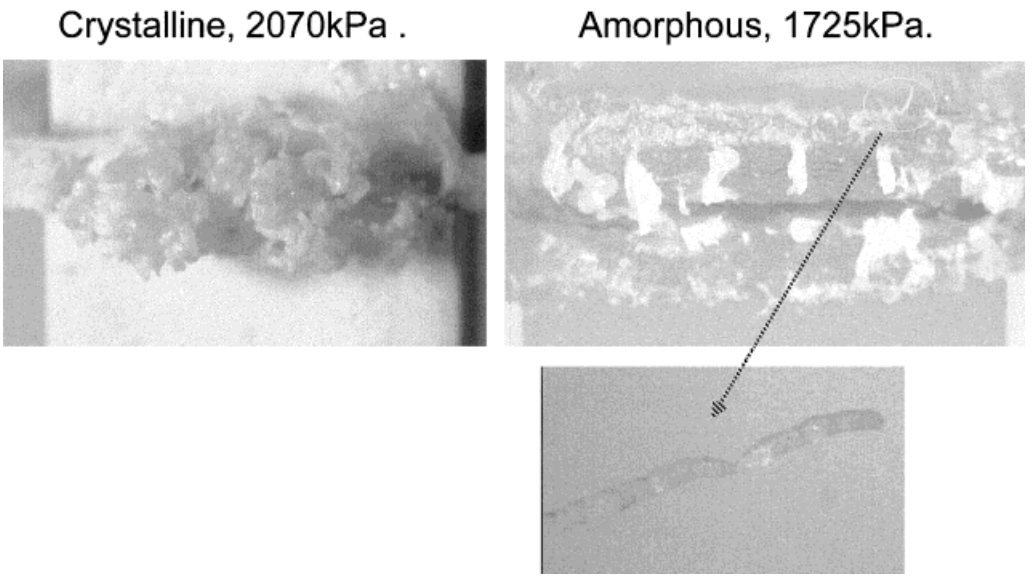

Figure 9 A weld extrudate picture showing macrofibrils. Welding conditions: frequency, 66 Hz; amplitude, 1.9 mm; 300 cycles.

procedure indicated earlier in Figure 3. This optical transmission photograph is shown in Figure 8. This image of the sample welded at 66 Hz (1.9 mm amplitude) with 690 kPa pressure at 50 cycles clearly indicate that once these regions start, the boundary between the HAZ and unaffected zone rapidly proceeds in the Z direction (the direction along which the normal pressure is applied). A closer inspection of these weld pockets reveal that these HAZ regions are composed of stratified alternating dark–light sublayers running parallel to the curved HAZ boundary. We have observed similar structural features in the shear crystallized regions of injection molded

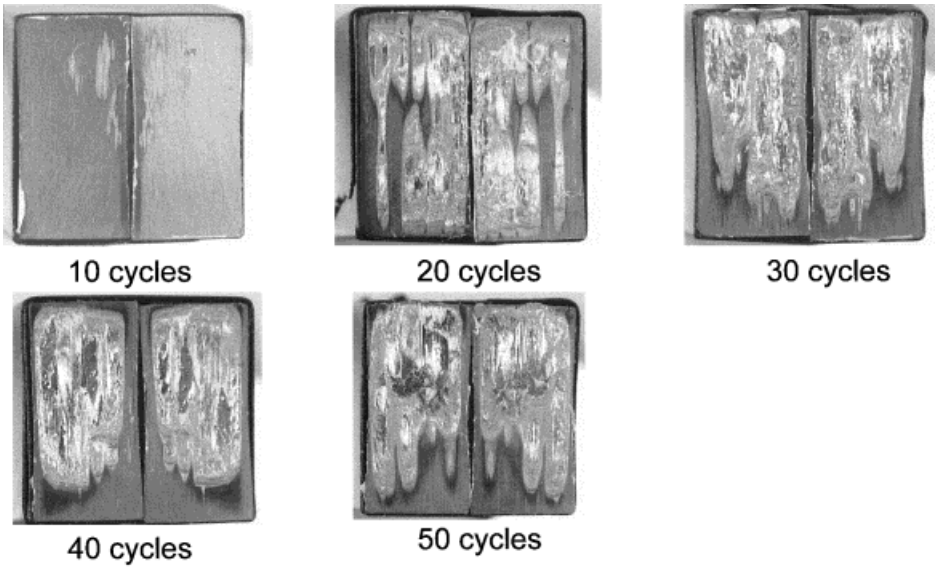

Figure 10 Time-sliced weld surfaces (after break): frequency, 66 Hz; amplitude, 1.9 mm; pressure, 689 kPa (100 psi); amorphous PEN.

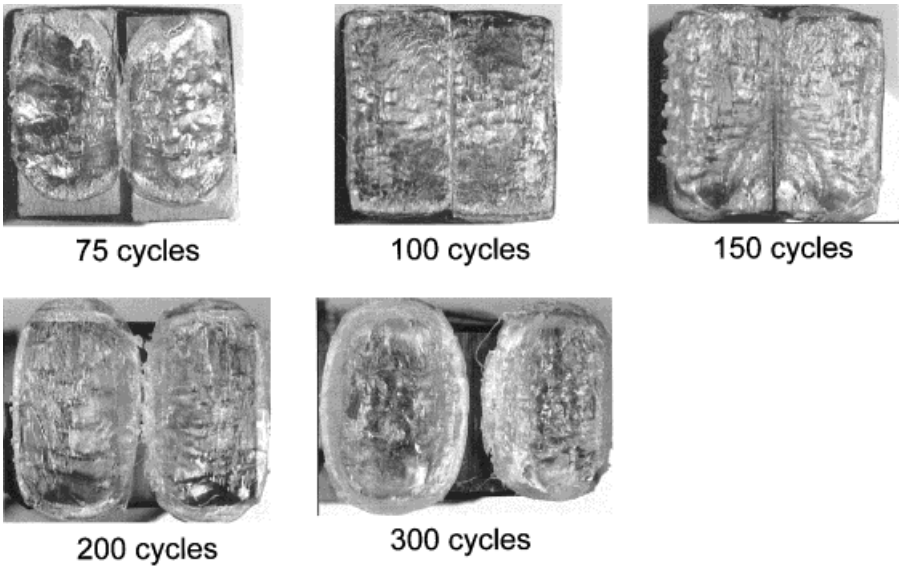

Figure 11 Time-sliced weld surfaces (after break): Frequency, 66 Hz; amplitude, 1.9 mm; pressure, 689 kPa (100 psi); amorphous PEN.

parts in an earlier study.[12] These layers may be a manifestation of the preferential alignment of the naphthalene planes upon stressing, which locally yield a series of alternating regions, most possibly as a result of oscillatory nature of the motion of the pieces relative to one another. In these images, the bottom piece oscillates in the direction normal to the paper plane, creating an oscillatory stress field as the material softening progresses away from the interface.

Another feature of the HAZ initiation mode can be observed in the extrudate (flash) pictures

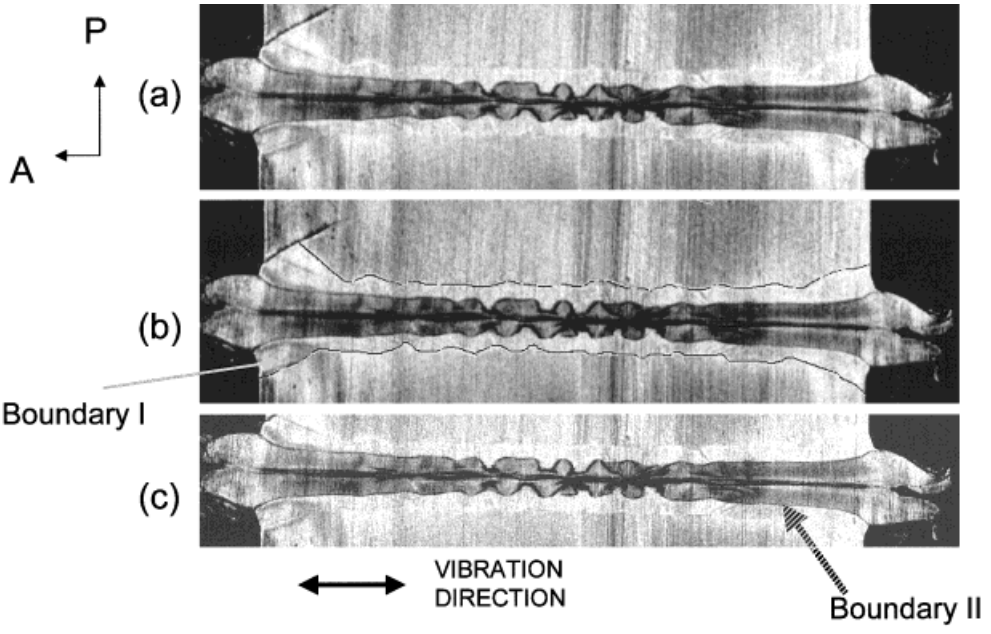

Figure 12 Transmission polarized optical micrograph of an amorphous sample welded at 66 Hz frequency, 1.9 mm; amplitude, 689 kPa (100 psi) normal pressure; 200 cycles; *X*–cut: (a) original image; (b) image traced with black + yellow line showing the first boundary (I); (c) image enhanced to highlight the second boundary (II).

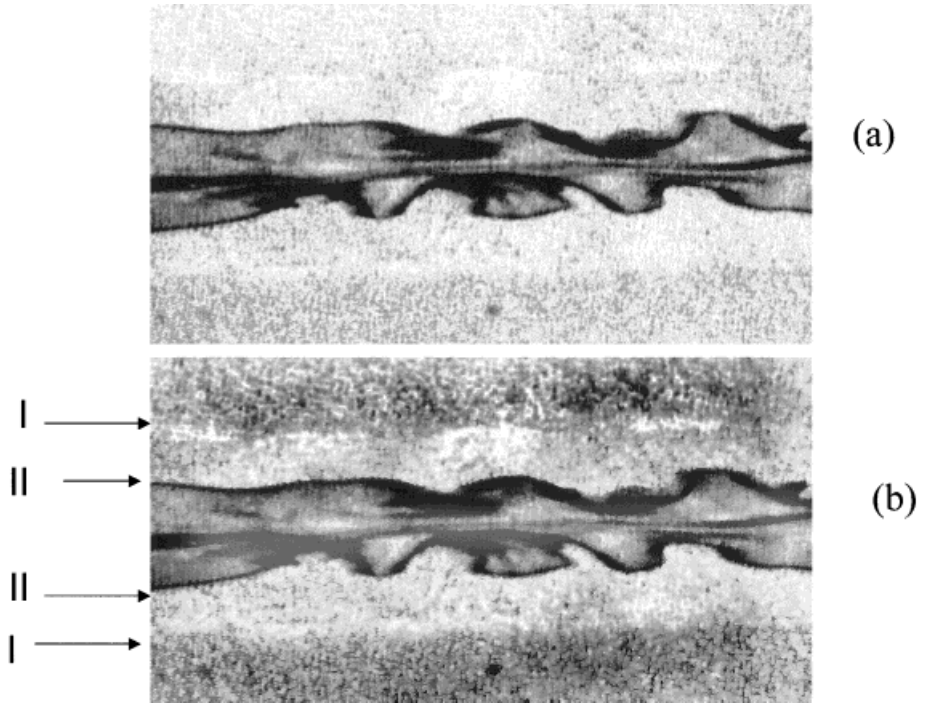

Figure 13 (a) Enlarged midsection of the sample in Figure 12. (b) image enhanced to show the 2 distinct boundaries.

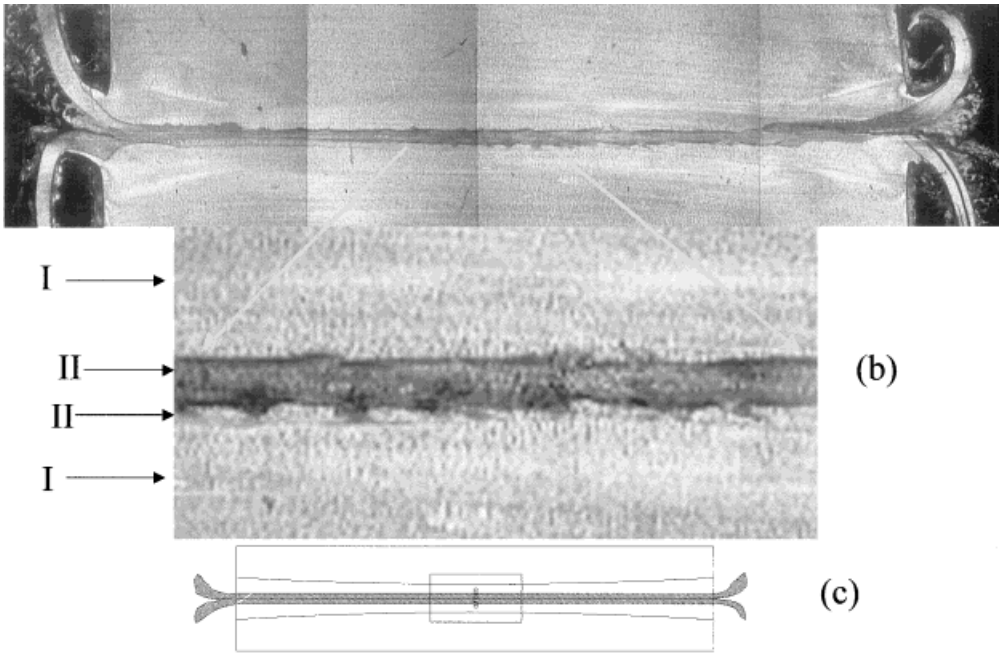

Figure 14 Optical micrograph of *X*-cut amorphous PEN (66 Hz frequency; 1.9 mm amplitude; 1035 kPa pressure; 300 cycles): (a) original image; (b) (enlarged and image-enhanced midsection showing wave patterns; (c) WAXS probe locations.

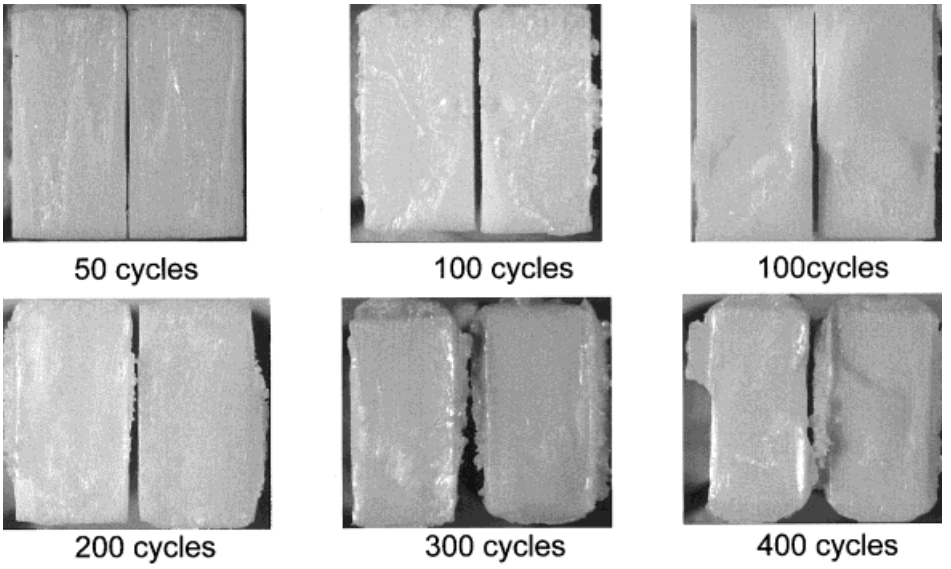

Figure 15 Time-sliced weld surfaces (after break) 66 Hz frequency; 1.9 mm amplitude; 100 psi pressure; crystalline PEN.

taken on the crystalline and amorphous samples shown in Figure 9. The material residing at the outer surfaces of the flash has come from the earliest times of the weld HAZ development, as they would be the first ones to be expelled from the interface. In these samples, large normal stresses were employed to generate a large amount of materials in the flash regions. The difference between the crystalline samples and the amorphous ones are rather clear in that the flash region in either one of these samples are not smooth. They are composed of rather nonuniform deformation fronts, particularly the crystalline ones, indicating that the processes that generated them have not taken place uniformly across the weld interface but originated from highly localized regions, which results in nonuniform flow front generated, as seen in the Figure 9. It appears that the rolled fibrillar particle generation observed at the early stages of welding is a result of the formation of highly localized weld initiation zones observed earlier. On closer inspection, these particles that reside at the top surface of the HAZ have a twisted appearance (see the magni-

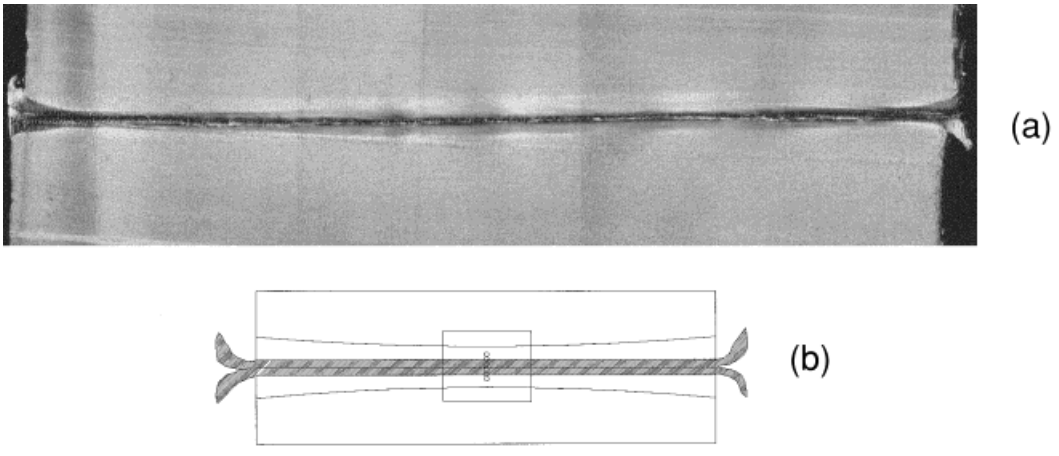

Figure 16 (a) HAZ of crystalline PEN welded with 66 Hz frequency, 1.9 mm amplitude, 690 kPa pressure; 300 cycles; 16× magnification. (b) Probing locations for micro-WAXS patterns.

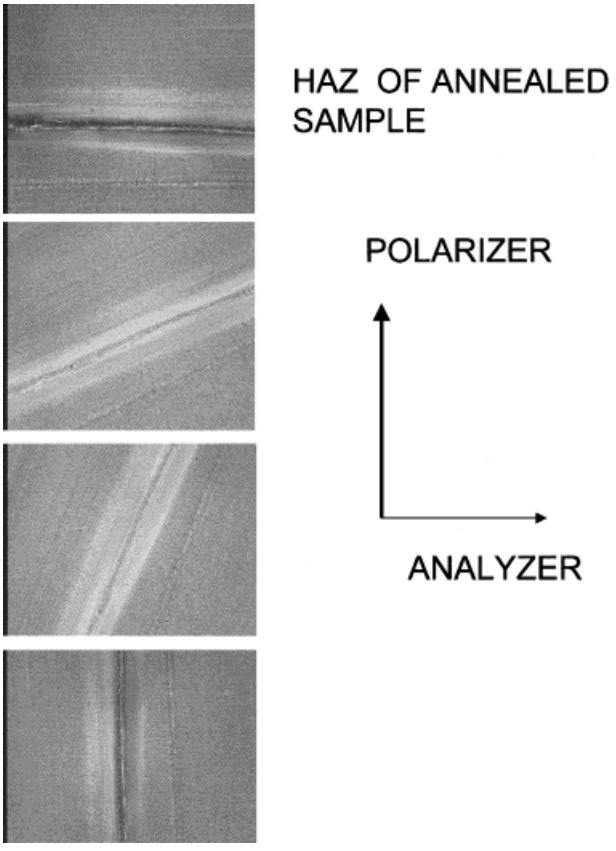

Figure 17 HAZ of crystalline sample at different directions with respect to the polarizer and analyzer.

fied example), indicating that they were rolled nonuniformly during the course of their expulsion from the interface. These rolled particles have been observed in other spin-welded polymers, such as polyvinylidene fluoride (PVDF), during the formation of the weld interface.[13] They are generally formed at an earlier stage at the front of the deformation zone in this process before the whole interface melts. It is also important to point out that these fibrillar formations are not observed in the crystalline sample flash. This is partly attributed to the elasticity of the deforming material generated during the course of the melting. For instance, once PEN is melted, it exhibits low melt viscosities,[8,11] and once molten, it generally exhibits low melt elasticity characteristic of most linear polyesters. Low viscosity combined with low melt elasticity generally results in a very low tendency to roll the particles in a nonuniform deformation field under normal pressure. This is what is suspected in the amorphous precursors since the temperature of the majority of the deformation field is in the rubbery range where the viscosities and melt elasticities are quite high, resulting in rolling tendencies of the particles that are ploughed from the melt pockets.

There appears to be two distinct stages for the evolution of interfacial features from amorphous precursors, as shown in Figures 10 and 11 for samples welded to systematically varying number of cycles at 66 Hz with 1.9-mm amplitude under 689-kPa normal pressure. The first stage extends from 10 cycles to about 75 cycles. In this stage, the interface melts nonuniformly, and the appearance of the long molten regions suggests that once a region is molten, it propagates in the direction of vibration first before its natural progression in the transverse direction takes place by the lateral coalescence of similar regions. In the second stage

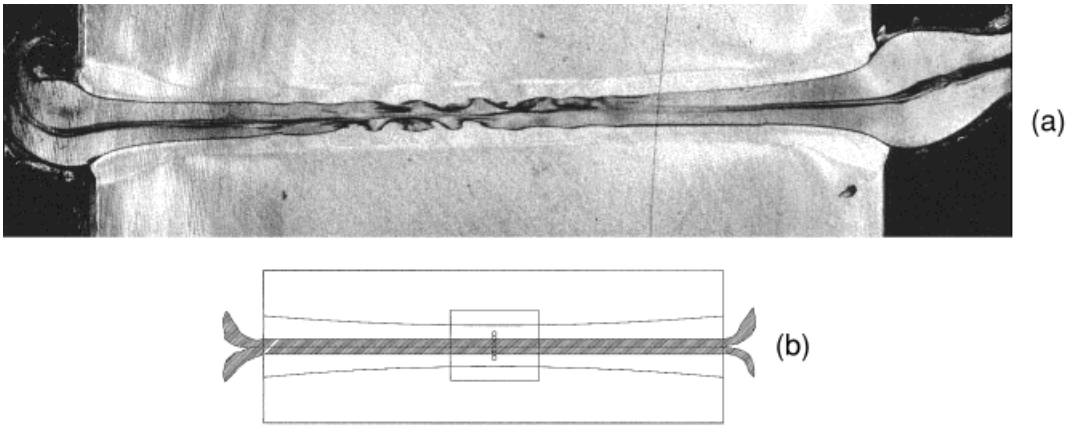

Figure 18 (a) Amorphous PEN, welded under 66 Hz frequency; 1.9 mm amplitude; 690 kPa; pressure, 300 cycles; 16× magnification. (b) Locations where the microbeam WAXS patterns were obtained.

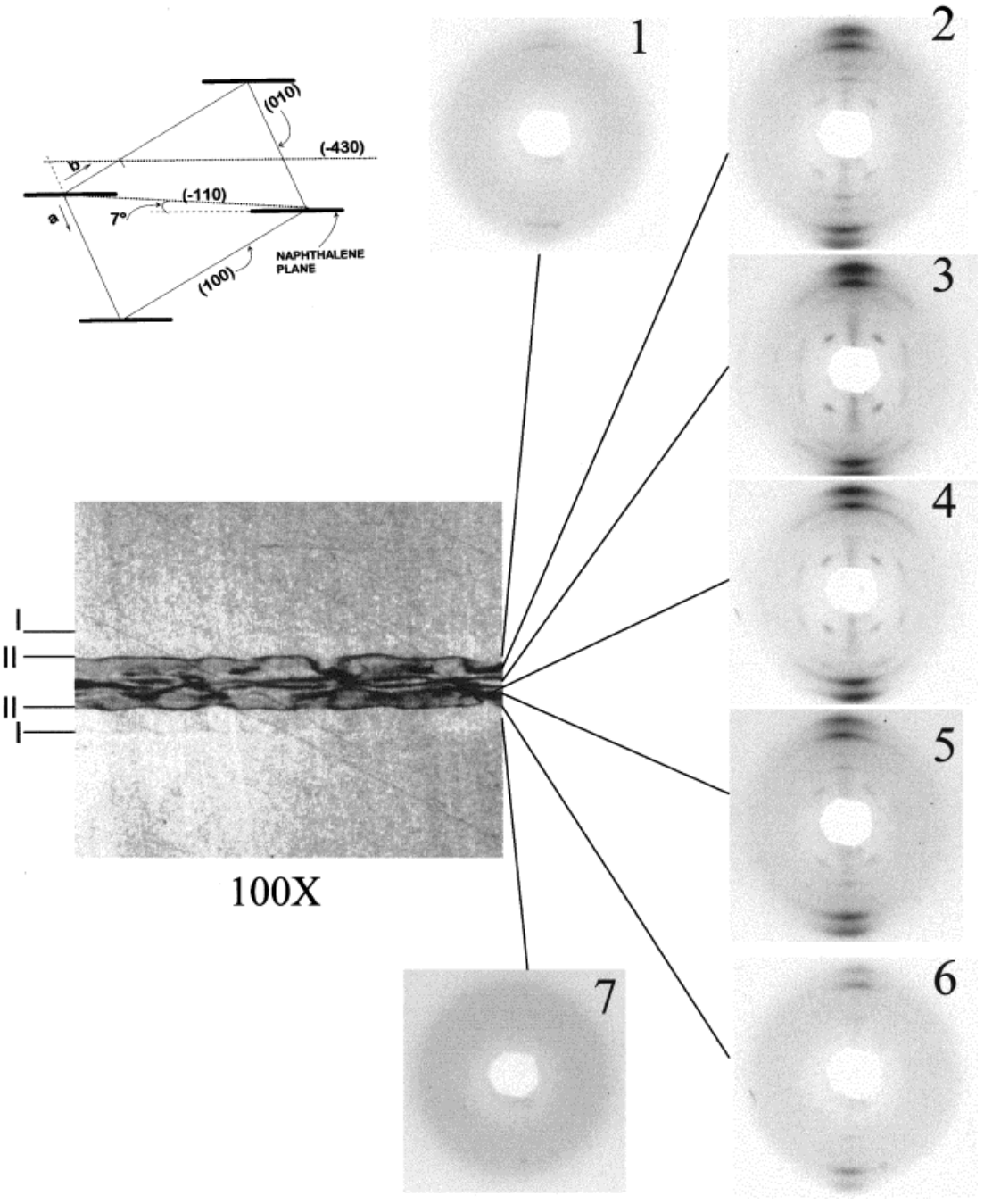

Figure 19a Microbeam X-ray patterns of amorphous PEN welded at 66 Hz frequency, 1.9 mm amplitude, 690 kPa pressure; 300 cycles.

starting around 75–100 cycles, a very distinct periodic ridges are observed in the direction of vibration. This is quite visible in sample surfaces from 100 to 300 cycles. In order to further investigate this phenomenon, we obtained an *X*-cut slice on a sample welded to 200 cycles shown in Figure 12(a). In this picture taken under cross polars, the long axis is along the vibration direction, and the short axis is in the direction of normal pressure, as indicated in the Figure 3. This HAZ is unusual in that it has 2 separate boundaries, I and II, shown in the image-enhanced pictures shown in Figure 12 (b) and (c). The wave pattern at the boundary II increases in

amplitude from the edge to the center of the sample, and the largest amplitude is observed at the center symmetry axis of the sample. In addition to this boundary, another boundary (Boundary I) is clearly observable in the unenhanced image shown in Figure 12(a). We traced this distinct boundary and found that it also exhibits an oscillating pattern and the peaks and valleys of these boundary spatially align with the peaks and valleys of the inner HAZ boundary II. This can be viewed in more detail in the magnified pictures of this region in Figure 13. This behavior is observable particularly in the upper boundaries I and II.

The increase of normal force not only causes the expected HAZ thickness reduction, but also the thickness of the heat affected zone, but causes a flattening of these wave patterns, as shown in Figure 14(b).

HAZ STRUCTURE EVOLUTION IN CRYSTALLIZED PEN

Fracture surfaces of the time sliced samples (66 Hz, 1.9 mm, 689 kPa), though exhibiting less contrast, show that the melting also starts at highly localized regions (see the picture of the sample welded with 50 cycle in Figure 15). However, the rest of the fracture surfaces are not as revealing as the first one. In these samples, the fracture did not always propagate through the heat-affected zone. This can be observed in the surface segments that exhibit a smooth fracture surface, indicating a brittle failure that has taken place through the unaffected regions out of the weld plane. In Figure 15, 2 samples are shown for 100 cycles to indicate variability of the fracture modes at this incomplete weld stage. In order to investigate the HAZ structure, as before, we sliced the sample with using *X*-cut procedure and observed it under cross polars shown in Figure 16(a). The HAZ thickness is much less than those that we observed in the amorphous samples. This is expected since interface has to reach temperatures 240°C and higher in order to deform; and for the same process conditions as the ones used for the amorphous samples, the temperatures reached at the interface will allow a smaller portion of the interface to melt. The second and very important point is that once the polymer reaches melt temperatures, it will be extruded much more readily under the same normal pressures, as it exhibits much smaller resistance to flow as compared to that of the rubbery amorphous material that is at

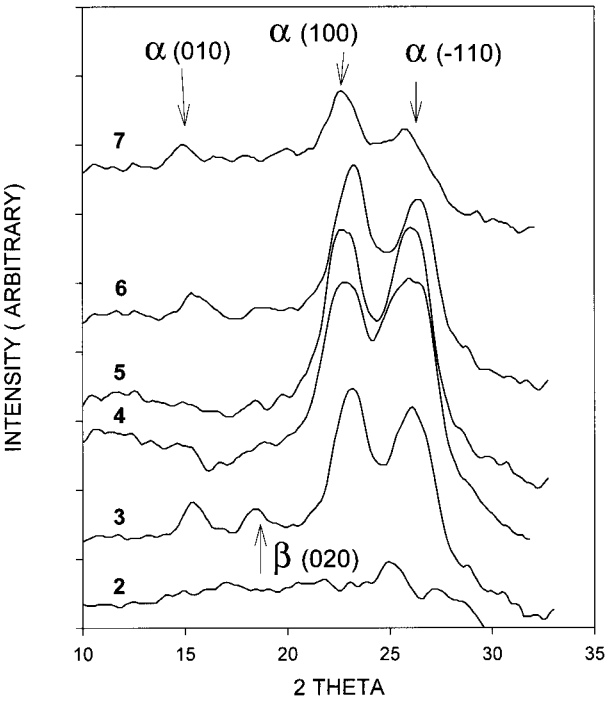

Figure 19b Equatorial scan of the WAXS patterns taken at the HAZ welded from amorphous precursors.

$T_g < T < T_m$ temperature range. Figure 16 also shows that the interface between the HAZ and the unaffected zone is a diffuse one in accordance with the melting temperature range shown in Figure 1. Figure 17 shows the close-up of the HAZ region at different orientations with respect to the polarizer and analyzer. When the mid-section of the HAZ becomes parallel to the polarizer or analyzer direction, it becomes darker, indicating that one of the principal axes of the refractive indicatrix is parallel to the weld plane. In these pictures, one can also note that the boundary between the heat-affected and unaffected regions is reasonably sharp. The orientation behavior of the interface is discussed in the next section.

ORIENTATION DEVELOPMENT IN HAZ

Wide-Angle X-ray Diffraction

In order to study the crystalline phase and orientation developed in the HAZ, we took a series of matrixing microbeam X-ray diffraction (MMBX) patterns at the center of the HAZ of samples welded from amorphous, (Figs. 18–20) as well as crystalline, precursors (Fig. 21). Approximate locations of these patterns taken with the X-ray beam normal to the

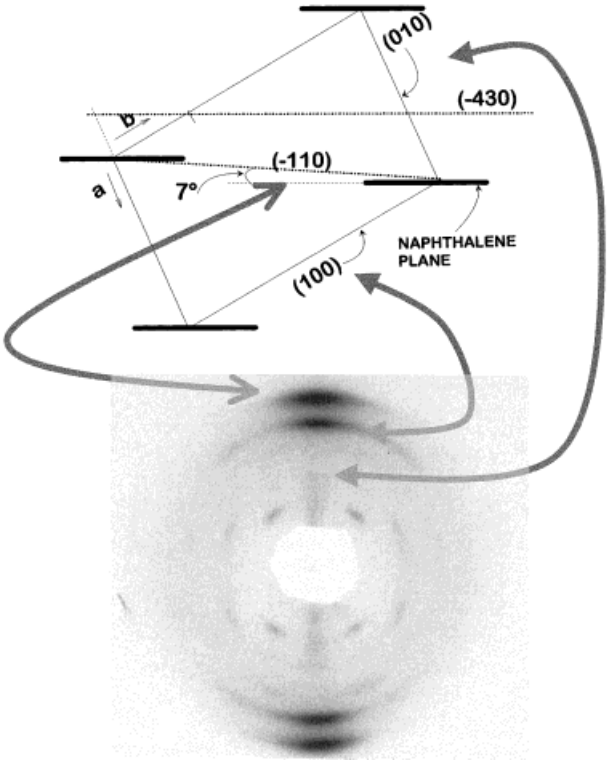

Figure 20 Identification of the crystalline planes in the α phase.

vibration direction (normal to the paper plane in these figures) are indicated in Figure 18 for the sample welded from amorphous state. Figure 19a indicates that the crystalline peaks are only observed between the inner two boundaries (II) and the patterns taken in the regions between boundaries I and outer boundaries I only show an unoriented amorphous halo. The WAXS patterns taken at numbers 1–6 mainly exhibit an α crystalline form, and all the equatorial planes are oriented in the direction perpendicular to weld plane (parallel to the normal force direction), indicating that the chain axes are aligned in the weld plane. On close examination of this data by taking equatorial (in these pictures, vertical) densitometric scans, (Figure 19b) it is revealed that not only the α crystalline form is present but also the β form (020) is present in the patterns 3, 4, and 5. This also confirms that the β form can be crystallized under high shear fields as seen in the injection-molded samples under specific conditions[8,11,12] as well as in the highly extensional deformation fields, as was observed in high-speed spun PEN[14] fibers.

Upon increasing the normal stress to 1035 kPa, the HAZ thickness decreases, and, correspondingly, the number of patterns where oriented crystalline peaks are observed is confined to the middle of this narrow HAZ bounded by the boundary I lines, as shown in Figure 21. It is noteworthy that the (010) plane intensities (indicated by the arrow in Fig. 20) are either very small or nonexistent at the number 4 and 5 locations in Figures 19 and 21. This is an important observation, indicating that the crystalline planes that contain naphthalene groups (−430) and (−110) [making 7° with (−430) align with their broad surfaces parallel to the shearing weld plane (Fig. 20)]. This is the reason the intensity of the (010) planes is low when the X-ray pattern is taken with beam directed normal to the long axis (vibration direction) of the sample.

Micro-WAXS patterns taken from the samples welded from the crystalline samples are shown in Figure 22. In the unoriented patterns of the number 1 and 5 locations, the polymer shows that the original polymer is in the α form, as expected since annealing the samples below about 220°C results in the α form. The β form is increasingly preferred if the annealing temperature is raised to temperatures ranging from 220–265°C.[15]

As indicated from the equatorial optical densitometric traces (Fig. 23) obtained from the WAXS patterns, the (010) planes are present in all patterns, and the β form (020) plane is absent from the equatorial regions of the pattern. These results indicate that the level of preferential naphthalene orientation and the chain axis orientation parallel to the weld plane is lower in the crystalline samples.

In order to quantify the orientation of the naphthalene planes, we have taken the azimuthal intensity distributions from the WAXS patterns and determined the $\langle \mathrm{Cos}^2 \chi\,(-110)\rangle$ for both the crystalline and the amorphous samples. Although we do not have a transverse isotropy in these, a sample as discussed above. It is more like a uniplanar axial texture (−430)[001], as found when PEN films are stretched in uniaxially,[16] as well as in shear crystallized regions of the injection-molded parts.[8,11,12]

Nevertheless, in order to make a quantitative comparison between the 2 types of samples, we determined the $\langle \mathrm{Cos}^2 \chi\,(-110)\rangle$ values and calculated the f [uniaxial orientation factor from just the poles of the (−110) planes] and plotted both values in Figure 24 for crystalline and as-molded initially amorphous samples. As was seen qualitatively in the WAXS patterns, quantitative results indicate that the HAZ regions of the sample

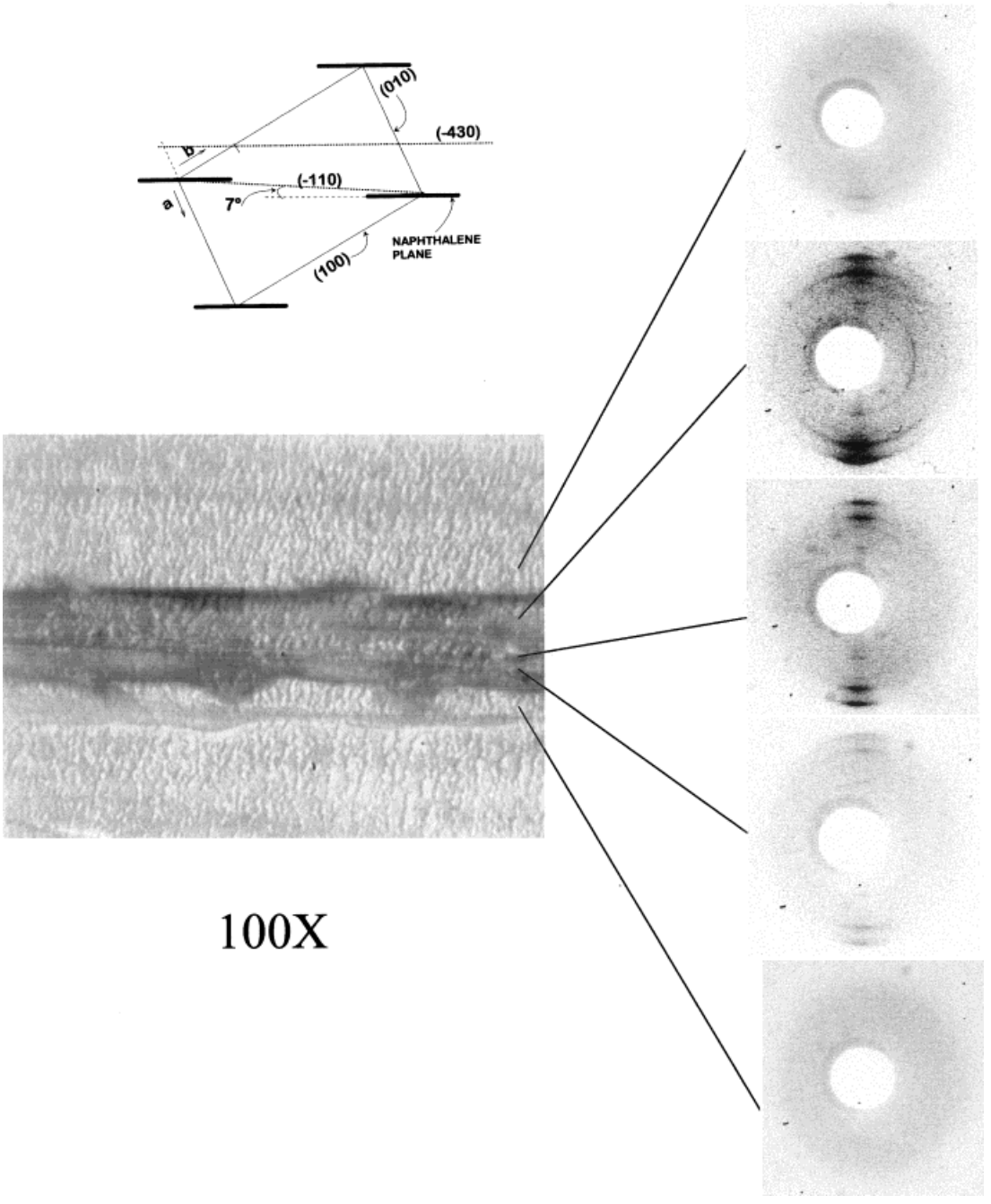

Figure 21 Micro-WAXS patterns for amorphous PEN welded under 66 Hz frequency, 1.9 mm amplitude, 1035 kPa pressure; 300 cycles.

welded from amorphous precursors is oriented to higher levels as compared to that from a crystalline precursor (annealed), despite the fact that the annealed sample exhibits a thinner HAZ region and lower viscosities at such high temperatures. In this graph, a value of 0 for $\langle \mathrm{Cos}^2\ \chi\ (-110)\rangle$ or the f value of (-0.5) indicate a perfect alignment of these planes in the weld plane.

High levels of orientation in the as-molded amorphous samples most probably is a result of higher stresses that has taken place in the HAZ of these samples during welding as the formation temperatures are much lower. As we will see in the next section, the preferential alignment of the naphthalene planes parallel to the weld interface is detrimental to the mechanical properties for the samples.

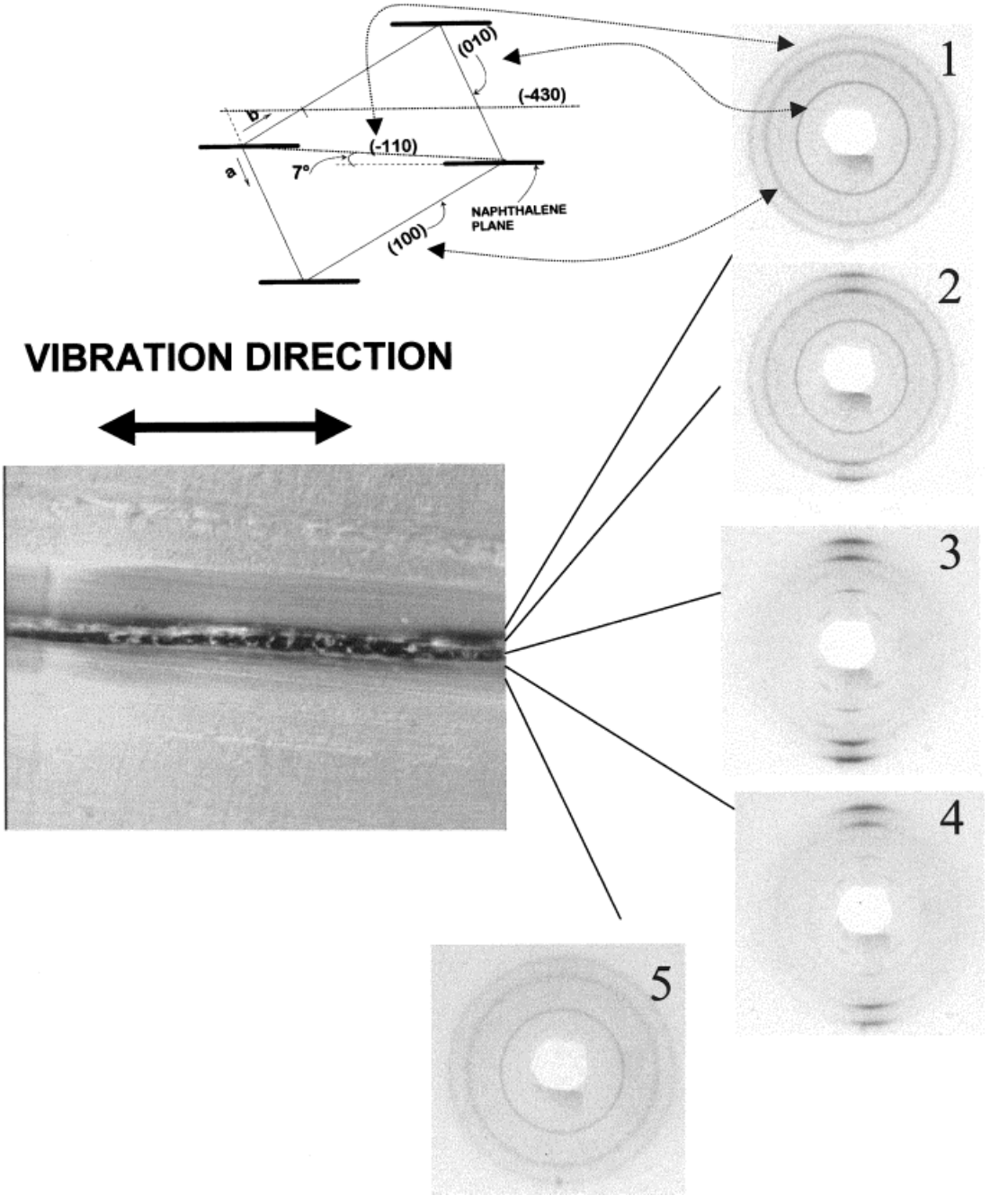

Figure 22 Microbeam X-ray patterns of crystalline PEN welded under 66 Hz frequency, 1.9 mm. Amplitude, 690 kPa pressure; 300 cycles.

Mechanical Properties

The break stress values for crystalline and amorphous samples are shown in Figure 25 as a function of the number of cycles they were subjected to during welding. After an initial increase, the values level off at about the same number of cycles (150–200), where the interfaces have completely melted. This occurs at higher number of cycles in the crystalline samples, as expected from the delayed melting in these samples. What is most striking is that the crystalline samples exhibit about twice the break strength as the amorphous ones. As discussed in the X-ray section, this is directly related to the naphthalene plane orienta-

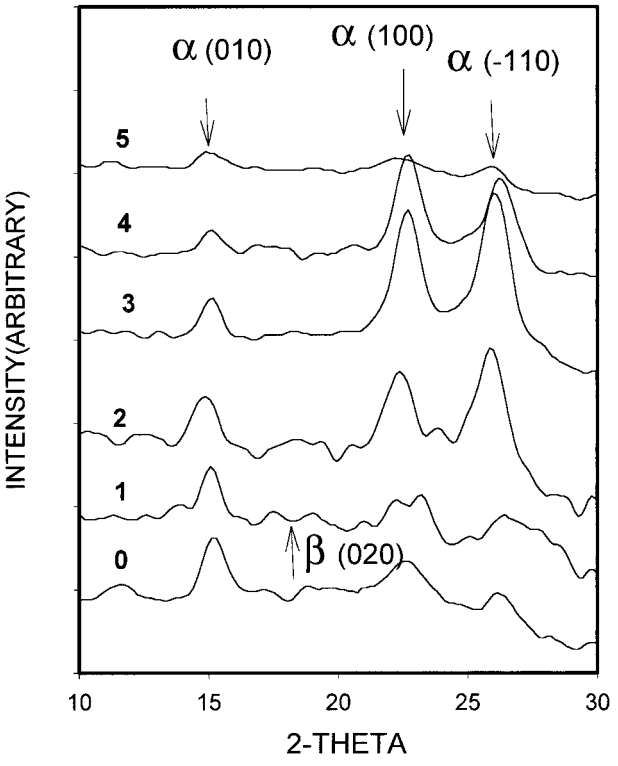

Figure 23 Equatorial scan of the WAXS patterns taken at the HAZ welded from annealed crystalline precursors.

tion at the weld interface. Lower temperature shearing results in higher levels of naphthalene orientation in the HAZ that is also much thicker in the initially amorphous samples. Because of the relatively low interchain forces between the naphthalene planes, this provides an easy cleavage plane across the HAZ. In fact, in all samples welded from amorphous precursors, the breakage occurred through the mid-weld plane. This is also evident in the fracture surfaces we have shown in Figures 10 and 11. These naphthalene plane orientation levels for crystalline samples are lower, and resulting strength values are higher. The fracture initiation and propagation does not always occur in the HAZ shown in Figure 15.

The increase in normal pressure increases the break stress up to a point in both types of samples shown in Figure 26, and a subsequent increase in normal pressure caused a reduction in break strength. This is easily attributable to the mechanism described above. It should be noted that the maximum in amorphous samples occurs at lower pressure levels as compared to the crystalline ones. Since the efficiency of preferential orientation is high in amorphous samples, the maximum is reached relatively early in order to obtain similar properties higher level of pressure is needed, as we have seen earlier.

CONCLUSIONS

It is clear from the experimental evidence presented in this article that there are significant differences in the welding behavior and resulting properties of PEN samples welded from amorphous or crystalline precursors. In order for the amorphous samples to deform, they need to be brought to temperatures just above the T_g (120°C for PEN), where the material behavior is rubbery, whereas the highly crystalline remains solid until the temperatures reach the start of the melting region located at about 240°C. As a result, under the same process parameters, the weld penetration starts in shorter times in the amorphous samples. Since the self-diffusion coefficients of the polymers in the rubbery state are rather poor due to the substantial viscosities, weld healing would not take place until the polymer is brought to the melting temperatures. This results in two HAZ boundaries across the weld. The inner boundary II is the demarcation point where the polymer has reached the melting range. The material that is in between the boundary I and II has reached the temperature between T_g and T_m during and im-

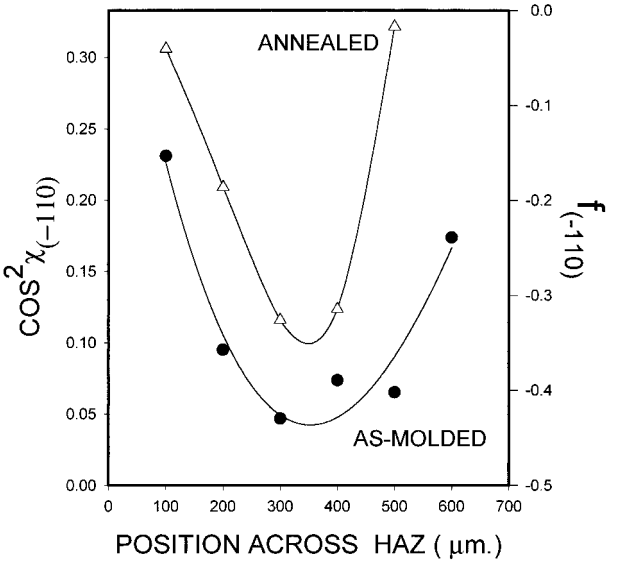

Figure 24 Orientation behavior of (−110) planes across the weld HAZ for annealed (crystalline) and as-molded (amorphous) parts.

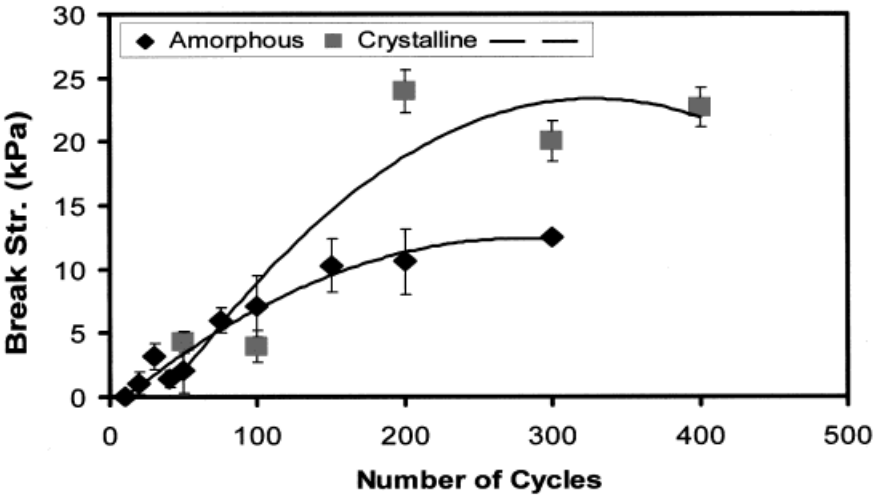

Figure 25 Break stress versus number of cycles. Weld conditions: 66 Hz frequency; 1.9 mm amplitude; 690 kPa normal pressure.

mediately after the welding process. Figure 28 basically shows the weld stages observed in amorphous PEN. It starts as a simple coulombic friction, and localized heating occurs, most possibly at local asperities that increase the local resistance to deformation. The localized molten material generated at this early stage acts as a local glue, which causes further localized heat dissipation that rapidly propagates the melting in the vibration direction. This results in elongated melt pools (stage II in the Figures 27 and 28). Once the interface is molten, a very distinct wave pattern emerges at the boundary I that separates the molten region from that of the rubbery region. The experimental observations clearly showed that the wavelength decreases while the amplitude increases towards the middle of the sample along the vibration axis of the sample. This phenomenon is as a result of two effects. One is the quite low melt viscosity exhibited by this polymer and relatively sluggish crystallizability of PEN. Once the polymer chains reach the melting temperature at the midplane, the heat generated is conducted away in both directions normal to the weld plane; this sets up a transient temperature gradient in both directions. Those regions that reach glass transition temperature are able to deform under the horizontal shearing forces and the normal forces, and boundary II observed is the demarcation line between the unaffected re-

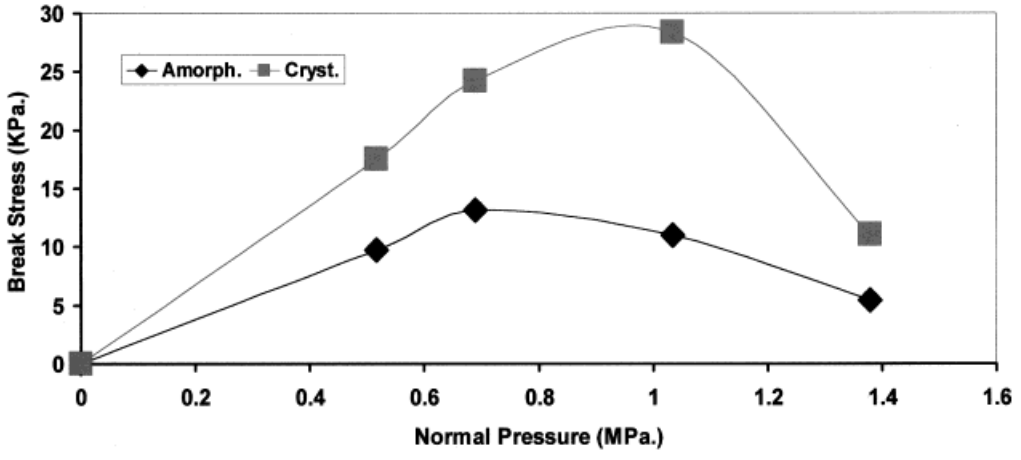

Figure 26 Break stress versus normal pressure for amorphous and crystalline samples welded under 66 Hz frequency and 1.9 mm amplitude; 300 cycles.

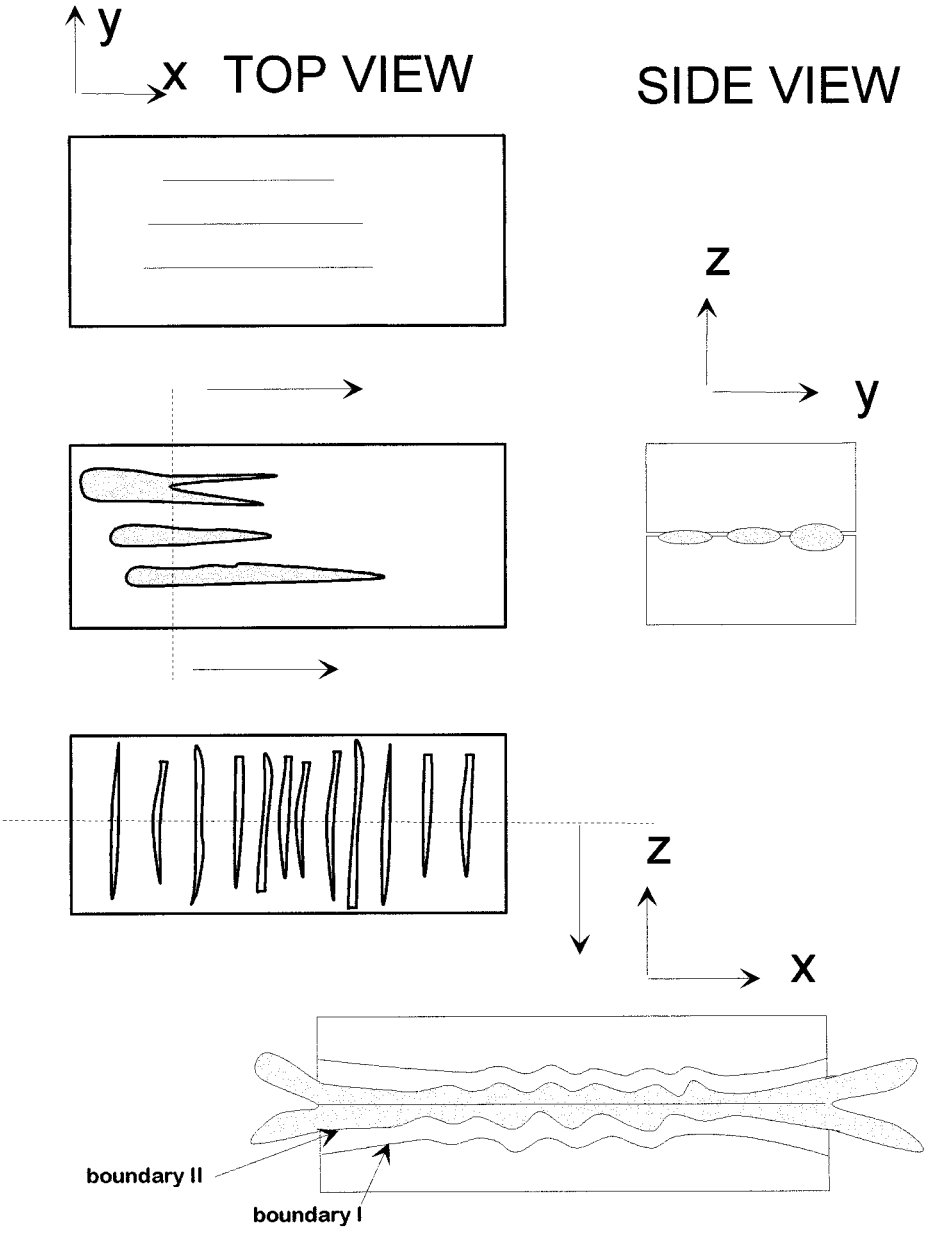

Figure 27 Idealized depiction of features observed in vibration welding of amorphous PEN.

gion (the region whose temperature did not exceed the glass transition temperature and the regions that did. We believe the sharpness of the boundary I is due to relative rapidity of the heating process that is not dissipated due to the naturally low thermal conductivity of the polymer. The wavy interface is due to the instabilities akin to the waves in the sea (the wind = low-viscosity medium blowing over the water = a high-viscosity medium). In our case, both media are presented by the same material in different states, with one being the rubbery state (water-equivalent) and the other I being the molten state (wind-equivalent). The striking wave patterns observed in the boundary II are, we believe, as a result of local variations of the thickness of the rubbery region (the region between boundary I and II) that causes boundary II to take its imprint as the material is heated by the heat flux conducted from the weld interface (heat generation source). Those regions that are closer to heat source (valleys in the boundary I) cause further penetration

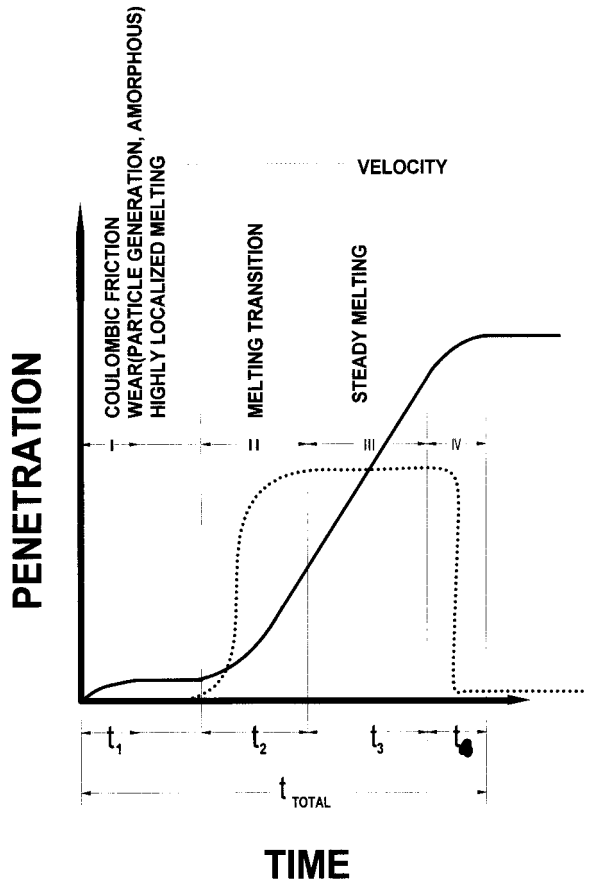

Figure 28 Weld phases of amorphous and crystalline PEN.

of the boundary II as compared to the regions that are away from the heat source (peaks in the wave pattern). This is quite evident in Figures 12 and 13.

In the interior of the HAZ (inside the boundary I), we observe high levels of crystalline orientation with the chain axes oriented parallel to the weld plane. The three-dimensional crystalline lattice structures are not fully established in these regions, as indicated by the absence of higher layer diffraction peaks. In these regions, the naphthalene planes, which are roughly parallel to the (−110) planes, are oriented parallel to the weld plane, while the chain axes are oriented parallel to the weld plane in the direction of the vibration. This is not unexpected since the material that has undergone a heating–cooling cycle during the welding also experienced significant shearing forces, which tend to orient the broad naphthalene planes roughly parallel to the weld interface. This gives rise of graphitic structure evolution at the interface that is rather splitty in character due to low interchain forces binding them together normal to the weld plane (in the direction of testing). As a result, this orientation behavior is detrimental to the mechanical properties and reduces the strength of the weld interface.

In samples welded from crystalline precursors, this orientation behavior is similar, but orientation levels were found to be less. As a result, these samples exhibit much higher weld strengths.

The authors thank Dr. Doug Callander of Shell Polyester Division for providing the PEN materials.

REFERENCES

1. V. K. Stokes, *Polym. Eng. Sci.,* **32,** 593 (1992).
2. V. K. Stokes, *Polym. Eng. Sci.,* **28,** 718 (1988).
3. V. K. Stokes, *Polym. Eng. Sci.,* **29,** 1310 (1989).
4. V. K. Stokes, *Polym. Eng. Sci.,* **28,** 998 (1988).
5. S. M. Stevens, *SPE Antec Tech. Pap.,* **42,** 1275 (1996).
6. S. Y. Hobbs and V. K. Stokes, *Polym. Eng. Sci.,* **31,** 502 (1991).
7. S. Schaible, M. S. thesis, University of Akron, OH (1992).
8. Y. Ulcer and M. Cakmak, *Polymer,* **35,** 5651 (1994).
9. Z. Mencik, *Chem. Prumysl.,* **17,** 78 (1967).
10. S. Buchner, D. Wiswe, and H. G. Zachmann, *Polymer,* **30,** 480 (1989).
11. Y. Ulcer and M. Cakmak, *Polymer,* **38,** 2907 (1997).
12. Y. Ulcer and M. Cakmak, *J. Appl. Polym. Sci.,* **62,** 1661 (1996).
13. S. Schaible and M. Cakmak, *Int. Polym. Proc.,* **10,** 270 (1995).
14. M. Cakmak and J. C. Kim, *J. Appl. Polym. Sci.,* **61,** 739 (1997).
15. S. W. Lee and M. Cakmak, *J. Macromol. Sci. Phys.* (in press).
16. Y. D. Wang, M. Simhambhatla, and M. Cakmak, *Polym. Eng. Sci.,* **30,** 721 (1990).